Contribution of Asian emissions to upper tropospheric CO over the remote Pacific

Linda Smoydzin[1] and Peter Hoor[1]

[1]Institute for Atmospheric Physics, Johannes Gutenberg University, Mainz, Germany

Correspondence: L. Smoydzin (smoydzin@uni-mainz.de)

Abstract. ~~We use CO data~~ By analysing the global distribution of the highest 2% of daily CO mixing ratios at 400hPa derived from the MOPITT satellite instrument ~~from~~ for 20 years (2000-2019~~to compose a climatology of severe pollution events in the mid- and upper troposphere over the northern-hemispheric (NH-~~), we detect very regularly regions with very high CO values (i.e. mixing ratios belonging to the globally highest 2%) over the remote northern hemispheric (NH) Pacific. ~~To link~~

~~each individual pollution event detected by MOPITT with a CO source region, we performed trajectory calculations using MPTRAC, a lagrangian transport model. To analyse transport pathways and uplift mechanisms we combine MOPITT data, the trajectory calculations and ERA-Interim reanalysis data.~~ ~~Events~~ Such events of elevated CO ~~which we detect at level between 500hPa and 300hPa over the~~ over the upper tropospheric NH-Pacific occur throughout the year, ~~occur~~ with a surprisingly high regularity and frequency (70% of all days during winter, 80% respectively during spring). ~~Our study further indicates, that the~~

~~spatial coverage of individual upper tropospheric pollution cluster increased in spring time during the 20 years we analysed.~~ ~~The position of upper tropospheric pollution plumes show a strong seasonal cycle.~~ During winter, most of these pollution events are detected over the north-eastern and central NH-Pacific, during spring over the central NH-Pacific and during summer over the western NH-Pacific. We detect most pollution ~~episodes~~ events during spring. ~~Trajectory simulations reveal China as the major CO-source region~~

To link each individual pollution event detected by the 2% filtering method with a specific CO source region, we performed trajectory calculations using MPTRAC, a lagrangian transport model. To analyse transport pathways and uplift mechanisms we combine MOPITT data, the trajectory calculations and ERA-Interim reanalysis data. It becomes apparent, that air masses from China being lifted along a frontal system into the free troposphere are the major CO source throughout the year. The contribution of other source regions and uplift mechanisms shows a strong seasonal cycle: NE-Asia in relation with upward transport of air masses in the warm conveyor belt of a midlatitude cyclone is a significant CO-source region during winter, spring and summer while India ~~and~~ is an important source region mainly during spring and summer and SE-Asia ~~are important source regions~~ mainly during spring.

1 Introduction

The long-range transport of trace gases and aerosols from East Asia across the Pacific has been subject of investigation for many years as pollution plumes can be lifted to the free troposphere where they are quickly transported to the North Pacific

and North American west coast by midlatitude storm tracks (Yienger et al., 2000; Liang et al., 2004; Holzer et al., 2005; Liang et al., 2005; Wuebbles et al., 2007; Turquety et al., 2008). A lot of effort has been spent in the last years to quantify the contribution of trace gases and aerosols of Asian origin to ~~north~~ North American pollution levels (e.g. Zhang et al., 2008; Yu et al., 2008; Hu et al., 2019; Yu et al., 2019). ~~Though~~ However, these studies mainly focus on the chemical processing of

30 the pollution plume rather than dynamical transport aspects. Several studies use satellite derived CO data to better understand vertical and horizontal transport mechanisms in relation to the prevailing synoptic situation. Ding et al. (2015) use data from numerical models and the MOPITT satellite instrument to investigate high levels of CO in the upper troposphere over the eastern Pacific while Liu et al. (2006) examine the influence of synoptic processes on the distribution of tropospheric CO also using MOPITT satellite data. Many studies in recent years focused on the role of the Asian summer monsoon anticyclone for

35 export of trace gases, pollutants or aerosols from Asia to the stratosphere or into the subtropical upper troposphere and tropical tropopause layer (e.g. Garny and Randel, 2016; Müller et al., 2016; Vogel et al., 2016; Yu et al., 2017; Santee et al., 2017; Lelieveld et al., 2018). Export of Asian pollution to the upper troposphere of mid and high latitudes however occurs at lower levels during the whole year. Numerous studies reveal a seasonal maximum of the Asian pollution outflow in spring. Studies, using CO as a pollution tracer explain this observation with efficient ventilation of the Asian boundary layer via midlatitude

40 cyclones and convection and increasing biomass burning emissions compared to winter (Liang et al., 2004; Holzer et al., 2005; Zhang et al., 2008; Yu et al., 2008; Luan and Jaeglé, 2013). Even though the strength and frequency of such pollution outflow events vary with season, they occur regularly throughout the year (Liang et al., 2004; Han et al., 2018). As stated by e.g. Liang et al. (2004), midlatitude cyclones seem to be the driving mechanism for long range transport (LRT) of polluted air masses from Asia to the western Pacific or north American west coast. More than half a century ago first studies reveal the existence

45 of air streams such as the warm conveyor belt (~~wcb~~WCB), cold conveyor belt and dry intrusion associated with extratrocpical cyclones. Since then, several studies investigate dynamical aspects of ~~wcb~~WCB's (e.g. Wernli and Davies, 1997; Wernli, 1997; Madonna et al., 2014; Gehring et al., 2020) as well as vertical transport of polluted air masses in warm conveyor belts in particular over the northern Pacific (e.g. Fuelberg et al., 2003; Kiley and Fuelberg, 2006; Klich and Fuelberg, 2014; Dickerson et al., 2007; Heald et al., 2003). Apart from uplift in the vicinity of a cyclone, orographic lifting (Chen et al., 2009; Ding et al.,

50 2009) and convection plays a major role for vertical transport of Asian pollution plumes especially during summer (Bey et al., 2001; Kiley and Fuelberg, 2006; Liang et al., 2005, 2007, 2004; Vogel et al., 2014).

Even though ~~wcb~~WCB's occur more frequent in the northern hemispheric winter than summer (Eckhardt et al., 2004; Madonna et al., 2014), their contribution to the uplift of polluted air masses is presumably important throughout the year (Liang et al., 2004). Madonna et al. (2014) find a global maximum of ~~wcb~~WCB's over the western North Pacific, China, and Taiwan during

55 NH summer. They discuss in detail that presumably a nearly stationary low-level baroclinic zone (Yihui and Chan, 2005; Ninomiya and Shibagaki, 2007) together with the East Asian monsoon, is responsible for tropical moisture exports over the west Pacific in summer explaining the high frequency of ~~wcb~~WCB's during June, July and August (Knippertz and Wernli, 2010). Generally, the Asian monsoon controls directly or indirectly the pollution outflow to the Pacific throughout the year (e.g. Kaneyasu et al., 2000; Müller et al., 2016; Lelieveld et al., 2018; Tomsche et al., 2019).

60 Many studies addressing long range transport of Asian pollution to the western Pacific or Arctic are based on case studies

(e.g. Heald et al., 2003; Di Pierro et al., 2011; Matsui et al., 2011; Roiger et al., 2011). Several of those studies see uplift in the vicinity of a cyclone as an important part of the pollution transport process though, those studies show very different, individual transport pathways across the Pacific. Luan and Jaeglé (2013) present a composite analysis of aerosol export events from Asia to ~~north~~ North America. Based on their analysis using MODIS satellite data and the GEOS-CHEM model, they find an enhancement of AOD values over the north-eastern Pacific/Alaska and over the south-western Pacific. The two separated maxima in the AOD composites appear as a split of the Asian outflow plume. Such a split of a single outflow plume caused by a blocking high pressure system over the Pacific is also described by Heald et al. (2003). Though in that particular case study, the northern branch of the plume reached the western US while the second branch headed southward towards the tropical western Pacific and no transport towards the Arctic was observed. Liang et al. (2005) and Reidmiller et al. (2010) also find that enhanced transpacific transport is characterised by the combined effects of a strong Pacific High and a strong low over Alaska. Even though many studies investigate the effect of long-range transport, they are mostly based on case studies like discussed above, use a composite approach or focus on meteorological conditions leading to uplift of polluted air masses into the free troposphere.

Our study presents a detailed analysis of the spatial and temporal distribution of elevated CO level as a pollution tracer in the mid and upper troposphere over the Pacific using 20 years of MOPITT data. We create a climatology of severe pollution episodes and use trajectory calculations to link each particular pollution event detected in MOPITT satellite data with a distinct source region. A second objective is the investigation of different uplift regions and uplift types, in particular ~~wcb-related~~ WCB-related upward transport. We analyse each trajectory linking a pollution event detected by MOPITT with a CO source region individually. We create a seasonal statistic about different transport pathways and uplift types depending on the location of elevated upper tropospheric CO, its source region, the uplift region and uplift type of polluted air masses.

2 Analysis of Satellite Data ~~and Model description~~

2.1 MOPITT

To detect pollution outflow events from the Asian continent, we use thermal infrared level 3 data from the version 8 product of CO measurements derived from the MOPITT instrument (Deeter et al., 2019). Level 3 products are available as daily mean values on a 1x1° global grid. The Terra satellite carrying the MOPITT instrument is flying in a sun synchronous polar orbit at an altitude of 705km. MOPITT splits the earth in pixels of a size of $22km^2$. By using a cross-tracking scanning method it sees the earth in a swath of about 640 km consisting of 29 pixels. A global coverage of the measurements would be reached after three days. Pixels with a high cloud content are filtered out. As MOPITT uses gas correlation spectroscopy of the thermal infrared radiation emitted from the earths surface, it can retrieve vertical profiles for almost two independent layers of CO. Data products are available on 10 level with a vertical resolution of 100hPa (surface, 900hPa - 100hPa). A retrieval algorithm is applied to the MOPITT data which is based on optimal estimation using a priori information to obtain additional constrains (Deeter et al., 2015).

2.1.1 ~~Method of data analysis~~

~~To be less dependant on the absolute number concentrations and related uncertainties of CO data derived from the MOPITT instrument (e. g.due to potential undetected slow drifts of the data over the 20 years of available data (Yoon et al., 2013)) and in order to capture only severe pollution outflow events from Asia, we select daily CO data~~

95

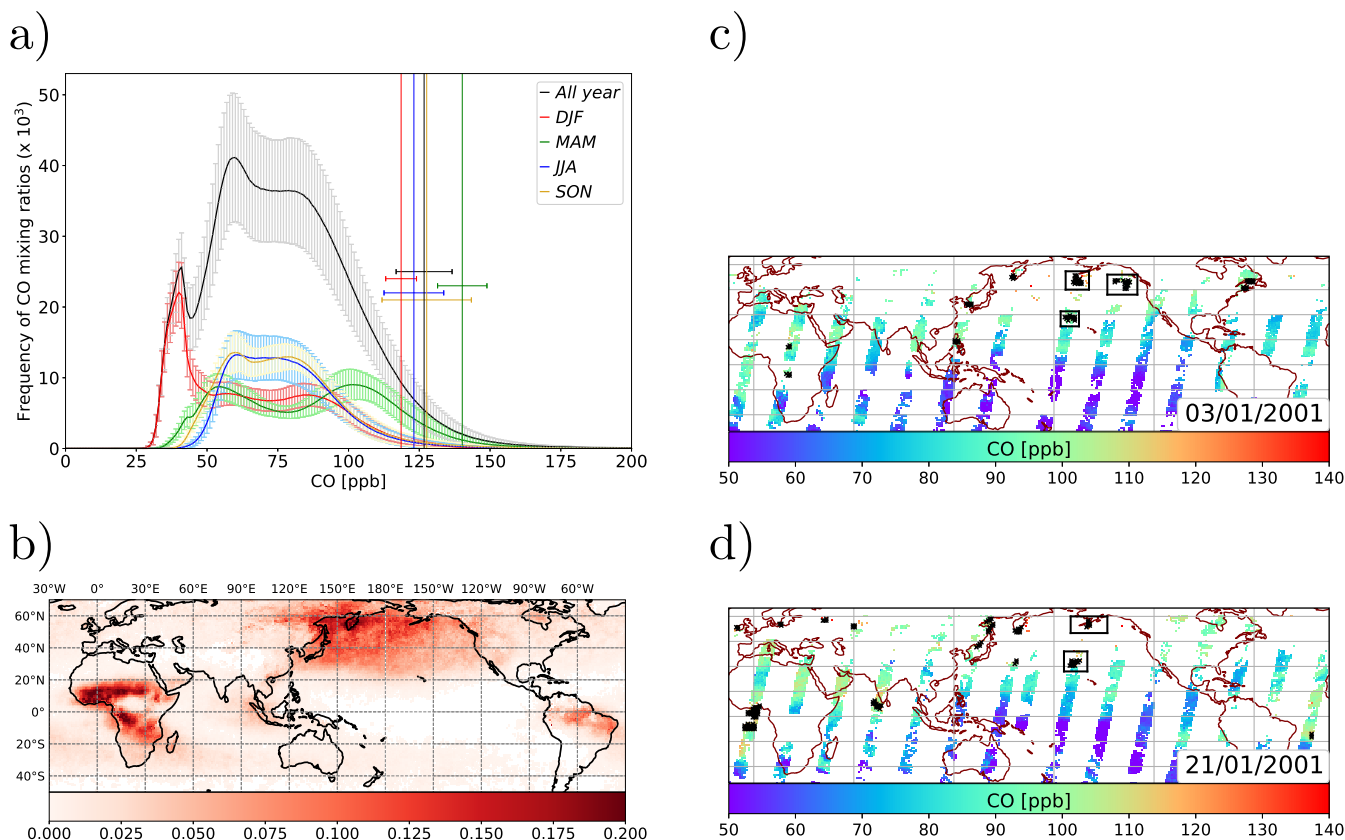### 2.2 Detection of long range transport events using MOPITT CO data

a)

c)

b)

d)

Figure 1. Fig. 1(a) shows the frequency distribution of mean CO mixing ratios [ppb] at 400hPa (years 2000-2019) as retrieved from MOPITT including the standard deviation. Vertical lines ranging from the bottom to the top of the plot denote the smallest (mean) mixing ratio, belonging to the highest 2% mixing ratios. Horizontal bars mark the standard deviation of this value. Fig. 1(b) shows the global frequency distribution (2000-2019) of the 2% data points (weighted with the total number of valid retrievals at each grid point).
Plots (c,d) show CO mixing ratios from one MOPITT overpath for two selected days. Black crosses mark the 2% highest CO values of the given overpath, which are selected. Black squares mark the CO maxima cluster where trajectories are initiated (section 3.1).

As we are primarily interested in upper tropospheric pollution episodes, we focus our analysis on the 400hPa data from MOPITT which is chosen as it is reliably in the troposphere throughout the year. The 300hPa level is frequently located above

the tropopause (north of about ∼45°) during winter (Wilcox et al., 2012) where CO mixing ratios decrease quickly. Note further, that the 400 hPa MOPITT CO has been shown to be insensitive to potential long-term bias drifts (Deeter et al., 2019), which could potentially affect long-term satellite observations (Yoon et al., 2013). To identify individual synoptic scale pollution events in the MOPITT CO data set, we determined a CO data set only focusing on CO anomalies of elevated CO as described in the following~~way: At each level, we only take into account those grid points with a mixing ratio belonging to the globally highest 2% mixing ratios (see example in~~: Daily CO data from MOPITT are highly episodic and variable. In addition, atmospheric CO mixing ratios generally undergo a seasonal cycle. Therefore, we use a statistical approach to select pollution events similar as Luan and Jaeglé (2013), who create a frequency distribution of modelled AOD values in a certain latitude range over the Pacific. This AOD distribution is log-normal and Luan and Jaeglé (2013) choose the top 20% days in the frequency distribution as LRT events. The frequency distribution of observed CO mixing ratios at 400hPa is also log-normal (Fig. 1~~, bottom row~~(a)) and we use the highest 2% of global daily CO data (literally spoken we cut off the left tail of the frequency distribution and only used the right tail, i.e. maximum 2% CO data) for our further analysis. Fig. 1(c,d) shows as an example all CO observations (from one overpath of Terra) at two selected days and the filtered grid points following the 2% criterion (black crosses). We refer to those data points as ~~CO-maxima~~CO maxima. Regions with at least three neighbouring maximum-grid points are defined as a CO-maximum cluster and are included in ~~or analysis.~~ our analysis. It turned out, that throughout the year, these CO maxima are found surprisingly regularly over the remote Pacific, far away from CO source regions and therefore, long-range transport of CO must be responsible for these observations (Fig. 1(b)).

It is hypothetically possible that on days with strong and widespread biomass burning at any region outside the studying region (i.e. the NH-Pacific), the pollution signal over the NH-Pacific is weak and we underestimate the number of severe pollution events. Though, due to the incomplete global coverage of the satellite data, MOPITT only sees a fraction of the potential biomass burning area (Fig. 1, (c,d)) such that a sufficient number of the selected 2% grid points is always located over regions which are not typical of biomass burning. In addition, it is possible that we miss LRT events where polluted regions are covered with clouds. However, on average we find 195 LRT events for winter (DJF) per year over the Pacific and respectively 330 for spring (MAM) per year, 239 for summer (JJA) per year, 98 for autumn (SON) per year (the Pacific region which is included in our analysis is shown in Fig. 3). The seasonal distribution of LRT events is very similar as the one found by Luan and Jaeglé (2013). Since the total number of events selected by our filter is rather large and certainly sufficient to compose a statistics, our final results regarding the trajectory analysis (section 3) would not be impacted severely if we missed single LRT events.

CO maxima events represent periods of elevated CO mixing ratios compared to background level. The difference between mean CO mixing ratios considering only CO maxima events and mean CO mixing ratios considering all data is rather high over almost the entire NH-Pacific during all seasons (Fig. 2). This indicates, that by our selection of data points we really capture periods with extraordinary high pollution level in the upper troposphere compared to background level. An exception is clearly visible over the northern Pacific during winter (Fig. 2, DJF) where the difference in CO mixing ratios is rather small and of no statistical significance. Thus we can assume, that the maximum CO-levels (according to our criterion) are within the variability of the climatological mean in this region during this time. They thus rather represent this mean than extreme
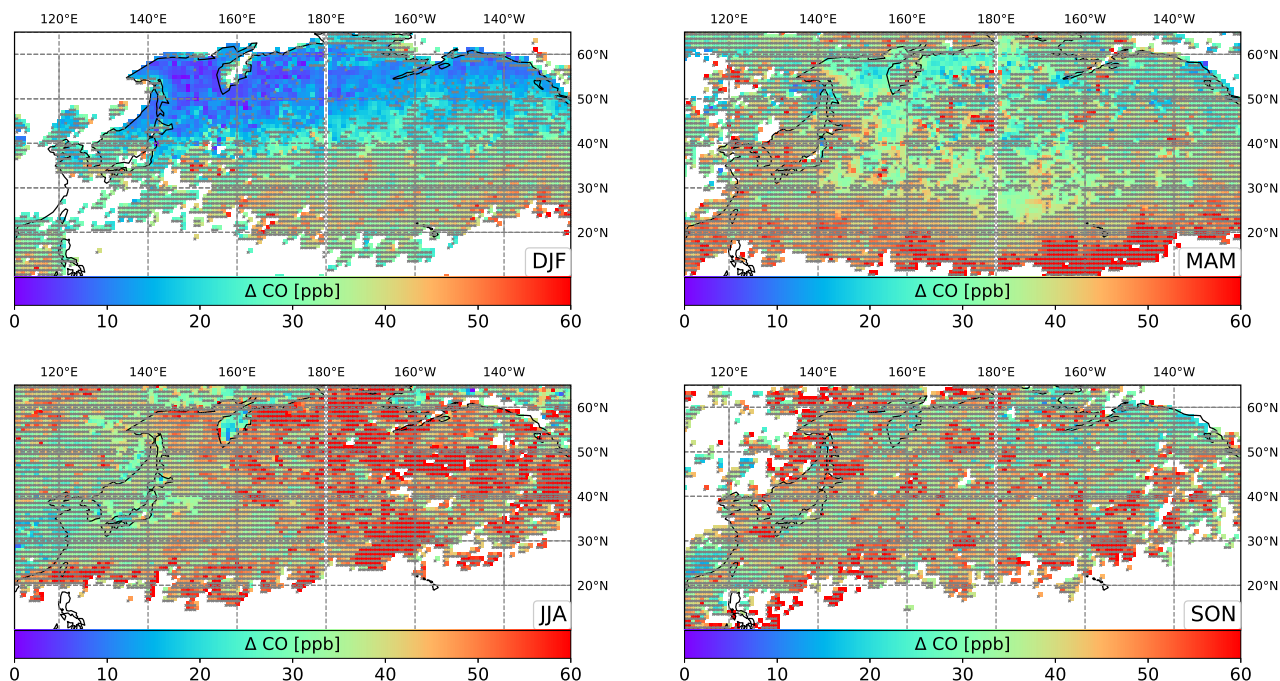
Figure 2. Difference (in [ppb]) between CO seasonal mean mixing ratios at 400 hPa considering only CO maxima events and total seasonal mean CO mixing ratios including all valid data points (2000-2019). Grid points which are marked by grey crosses have a difference with a strong statistical significance (regions where the pooled standard deviation is within a 99% confidence interval).

135   pollution events. This conclusion can also be drawn for the central NH-Pacific during spring (Fig. 2, MAM). Regions with a difference in CO mixing ratios of low statistical significance are also found during summer east of Japan (Fig. 2, JJA) where many maxima events occur. Though, this region is much closer to potential CO sources than the northern/central NH-Pacific (where background CO level are lower) and it is less surprising that pollution outflow events strongly impact the overall climatological mean at this site.

140   CO maxima events occur throughout the year over the NH-Pacific with autumn showing an exception with much less events than during the rest of the year (Fig. 3). A seasonal shift of the regions where most CO maxima occur at 400hPa is clearly visible (also at 500hPa and 300hPa). In winter time (Fig. 3, DJF), CO maxima occur more often over the north-eastern NH-Pacific while they are found over the central NH-Pacific during spring (Fig. 3, MAM). The total number of CO maxima events is much higher during spring than in other seasons which is in agreement with other studies showing a maximum of pollution export

145   from Asia during spring (e.g. Luan and Jaeglé, 2013; Holzer et al., 2005; Zhang et al., 2008; Yu et al., 2008; Liang et al., 2004) . During summer time (JJA) the occurrence of midlatitude cyclones is generally less frequent than during winter and spring while convection and the Asian summer monsoon gain in importance as transport pathways. The detected CO maxima are then found much closer to the continent over the western NH-Pacific, Siberia and Kamchatka.

We detect CO maxima over the NH-Pacific on ∼70% of all days during winter and summer, ∼90% during spring and ∼40%
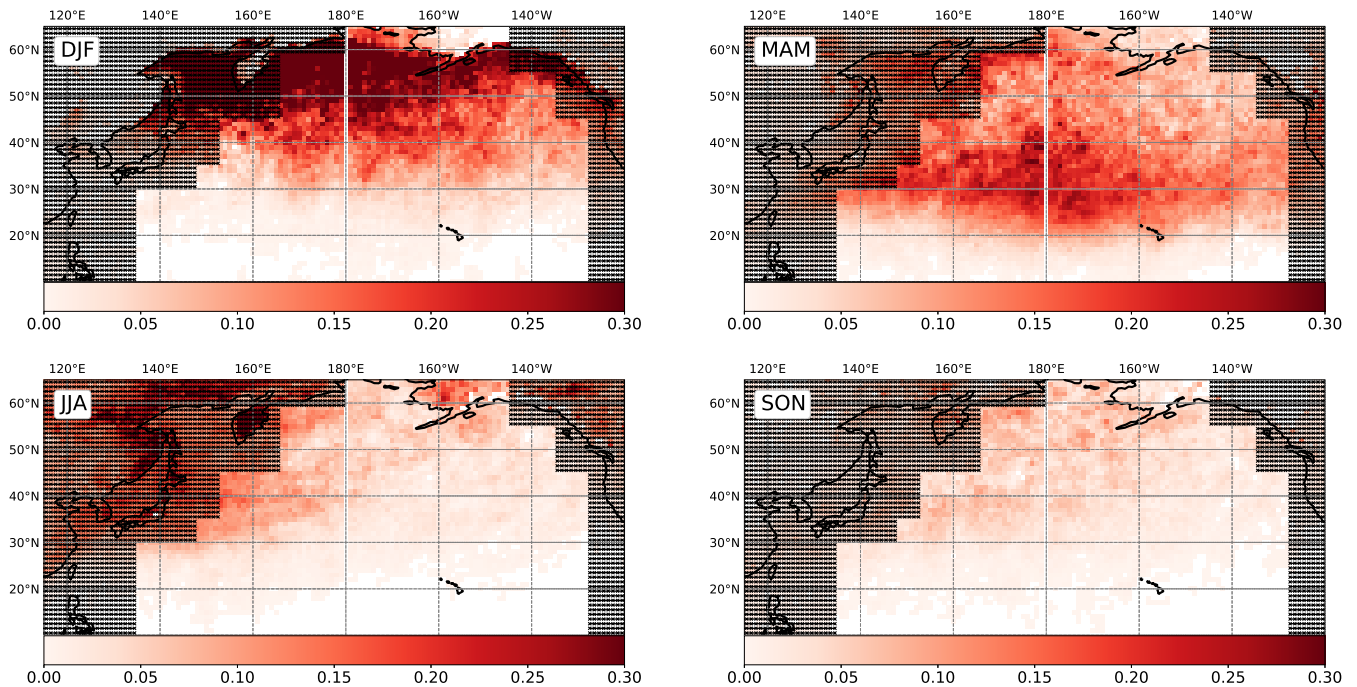
Figure 3. This plot shows the same quantity as Fig. 1b) though, separately for each season and solely for the Pacific region (i.e.: the global frequency distribution (2000-2019) of the 2% data points weighted with the total number of valid retrievals at each grid point). Only CO maxima in the area which is not grey-shaded is included in the trend- and trajectory analysis.

of all days during autumn (Fig. 4 (C)). The high temporal frequency of LRT events during spring stays unchanged during the analysed time period while the number of CO maxima days decreases from 2000 until 2019 in winter, summer and autumn. Though, the linearity (and therefore the trend) of the data set is rather weak.

The daily number of grid points which are selected by our filtering method as a CO-maximum over the Pacific varies strongly (visible in the high standard deviation, Fig. 4 (A)). We select exemplarily 84 grid points in total on 03.01.2001 (46 are located over the study region over the Pacific, distributed among three cluster Fig. 1 (c)) and 131 grid points on 21.01.2001 (24 grid points are over the Pacific, distributed among two cluster, Fig. 1 (d)).

During the 20 years of daily data, which we analysed, the number of CO maxima grid points slightly increases during spring (slope of regression line: 0.14) and decreases during winter (slope: -0.12, Fig. 4 (A)) while the number of cluster (Fig. 4 (B)) and the frequency of LRT events (Fig. 4 (C)) stays the same (slightly decreases for winter). Both trends (MAM, SON) are small but mathematically of statistical significance. Though the results need to be carefully interpreted. At first, the standard deviation of the mean number of CO maxima grid points found in one season is very high (especially for spring). Secondly, we cannot directly conclude, that the spatial coverage of severe pollution episodes increased, though it is likely. Regarding our filtering method, an increase of the number of CO maxima grid points over the Pacific during spring could hypothetically be also the result of e.g.: (i) weaker biomass burning in other regions of the world, (ii) CO emission reductions in other regions
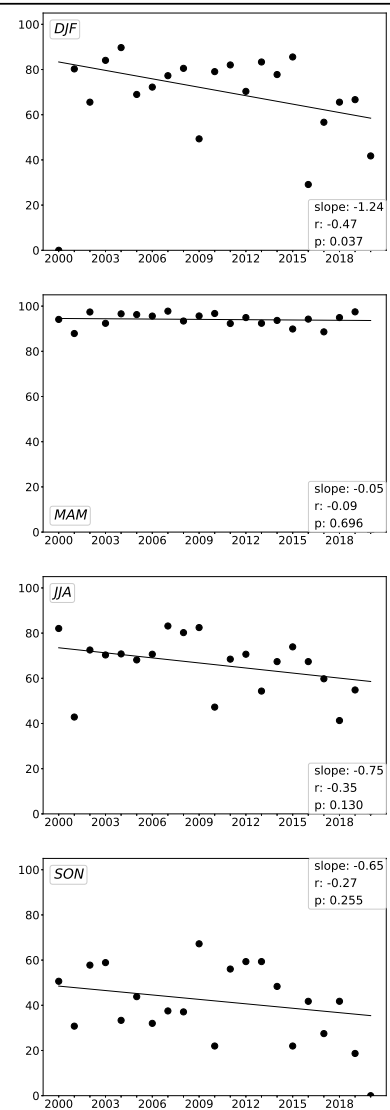
7
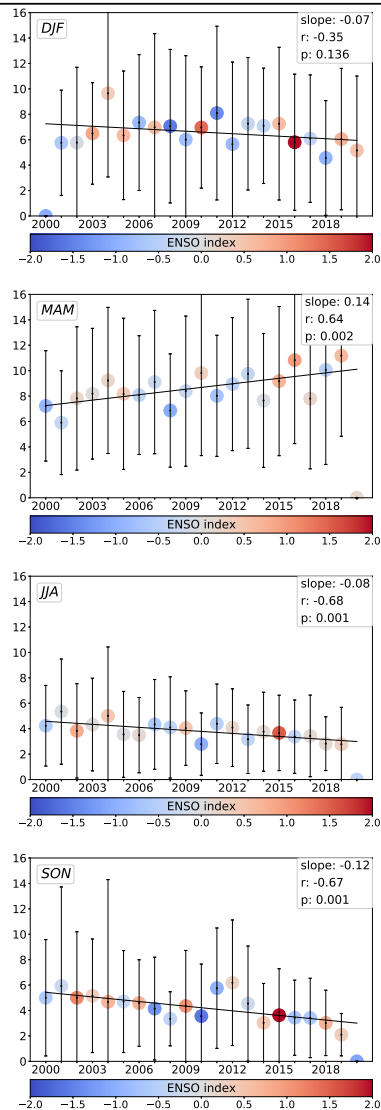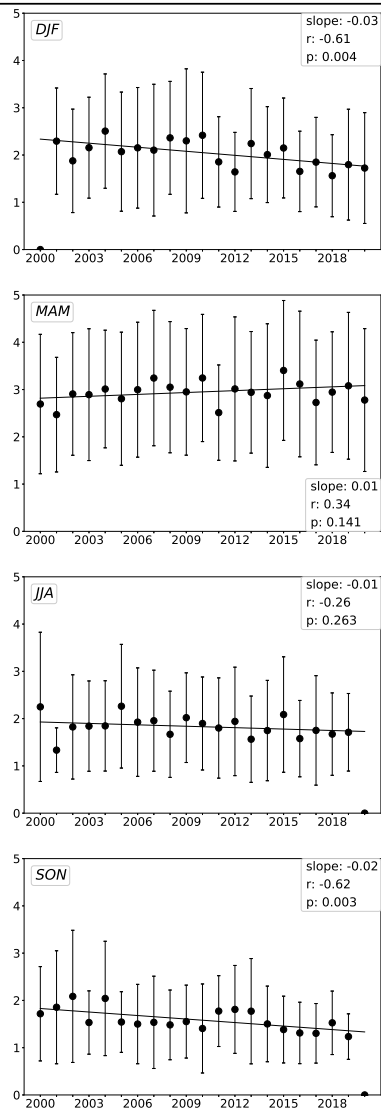
Figure 4. Plots show time series of the season mean number of daily CO maxima grid points, normalised with the total number of retrieved MOPITT data points (A) over the NH-Pacific. Circles are coloured with the ENSO index (taken from https://www.cpc.ncep.noaa.gov/products). Vertical lines show the standard deviation of the daily number of CO maxima grid points with respect to the season mean. Further shown is the season mean number of CO maxima cluster (B) and the percentage of the number of CO maxima days within one season, weighted with the number of days with MOPITT data (C). The area, which is included in this analysis is shown in Fig. 3. Periods with data gaps are excluded from the statistics.
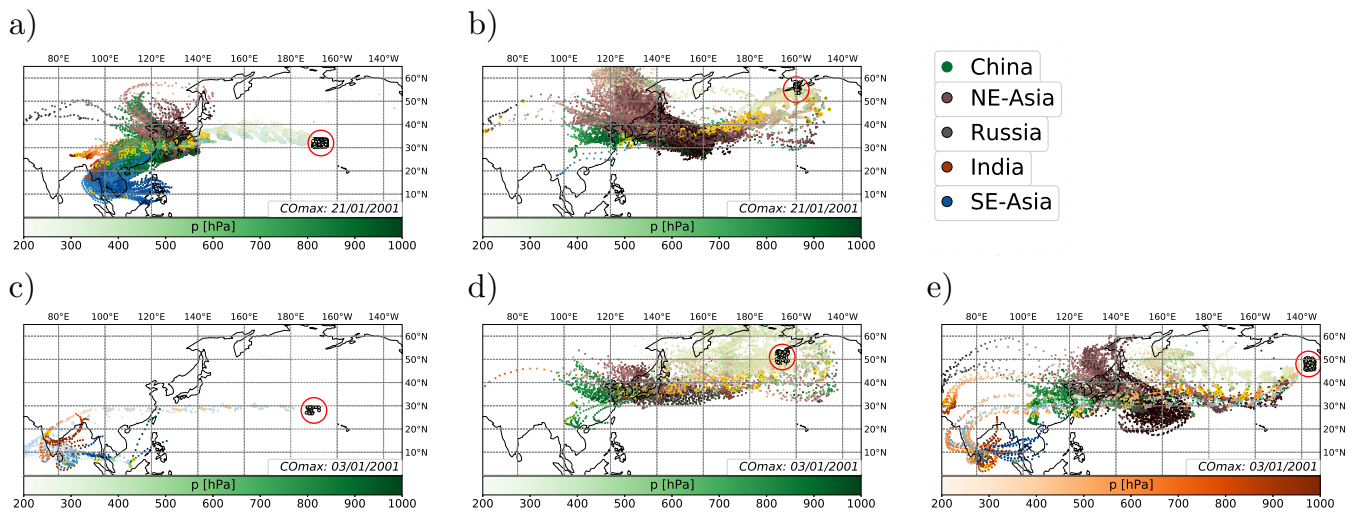
Figure 5. Plots show trajectories starting at a CO maxima cluster on 03.01.2001 (lower row) and 21.01.2001 (upper row). Trajectories with the same source region, have the same colour (see legend, e.g. trajectories from China are green, those from SE-Asia blue). The lighter the col-our of the circles marking the position of the trajectory, the lower the pressure level. Yellow circles mark the time of uplift, black circles (over the Pacific) mark the start position of the trajectories, i.e. the region of the CO maxima cluster.

of the world, (iii) a faster dilution of CO plumes in other regions of the world, (iv) less clouds over the Pacific or more clouds over other polluted areas or (v) instrumentational reasons. In addition, it is well known that precipitation patterns over the Pacific and the position of the jet stream can be altered during El Niño episodes (Breeden et al., 2021), and thus transport pathways of pollution plumes. Therefore, we considered a correlation between warm phases of ENSO and our selected LRT events. Years with an extraordinary large spatial extension of the upper tropospheric CO maxima cluster during MAM (e.g. 2004, 2010, 2016, 2019) are indeed related with El Niño periods (Fig. 4 (A)). This result is in agreement with the work by Breeden et al. (2021) who find an increase in storm track activity during La Niña years compared to neutral or El Niño years. Nevertheless, the changes over time (2000-2019) concerning the selection of LRT events are small compared to the large total number of LRT events selected during the 20 years of available MOPITT data by our 2% filter criterion. Therefore, these changes do not impact the trajectory analysis significantly which is presented in section 3.

3   Trajectory analysis

3.1   MPTRAC

In order to link the regions of elevated CO derived from MOPITT with a particular source region, we use the trajectory model MPTRAC (Hoffmann et al., 2016) which was recently developed at the Jülich Supercomputing Centre. MPTRAC is a massive-parallel lagrangian particle dispersion model allowing a computationally efficient calculation of transport simulations in the

troposphere and stratosphere.

We calculate backward trajectories starting in a square region covering each single CO-maximum cluster detected by MOPITT. To account for the vertical extent of the averaging kernel and uncertainties in the reanalysis data set driving MPTRAC, trajectories are initiated at 400hPa with a random variation of this altitude between 386hpa and 424hpa. The number of trajectories for each square covering a CO-maximum cluster is defined by $(\Delta \text{lon} * \Delta \text{lat}) * 100$. Trajectories are started four times a day (00 UTC, 06 UTC, 12 UTC, 18 UTC) if a CO-maximum was observed. The simulation time is 16 days. Meteorological input data for all trajectory calculations are taken form the ERA-INTERIM data set (Dee et al., 2011). Output is also written every six hours in order to compare our MPTRAC simulations with the ERA-INTERIM data set. Trajectories are included in our statistics if they descend below 850hpa, altitude above ground is less than 1.5km and if trajectories cross emission regions (taken from the IPCC AR5/RCP85 emission inventory (Lamarque et al., 2010)) with a CO flux of at least 0.1×10^{-9} kg(CO)/m^{2}s. This value roughly corresponds to an average CO emission flux in industrialised regions excluding biomass burning emissions. As a reference for CO emissions we use the IPCC AR5/RCP85 emission inventory (Lamarque et al., 2010).
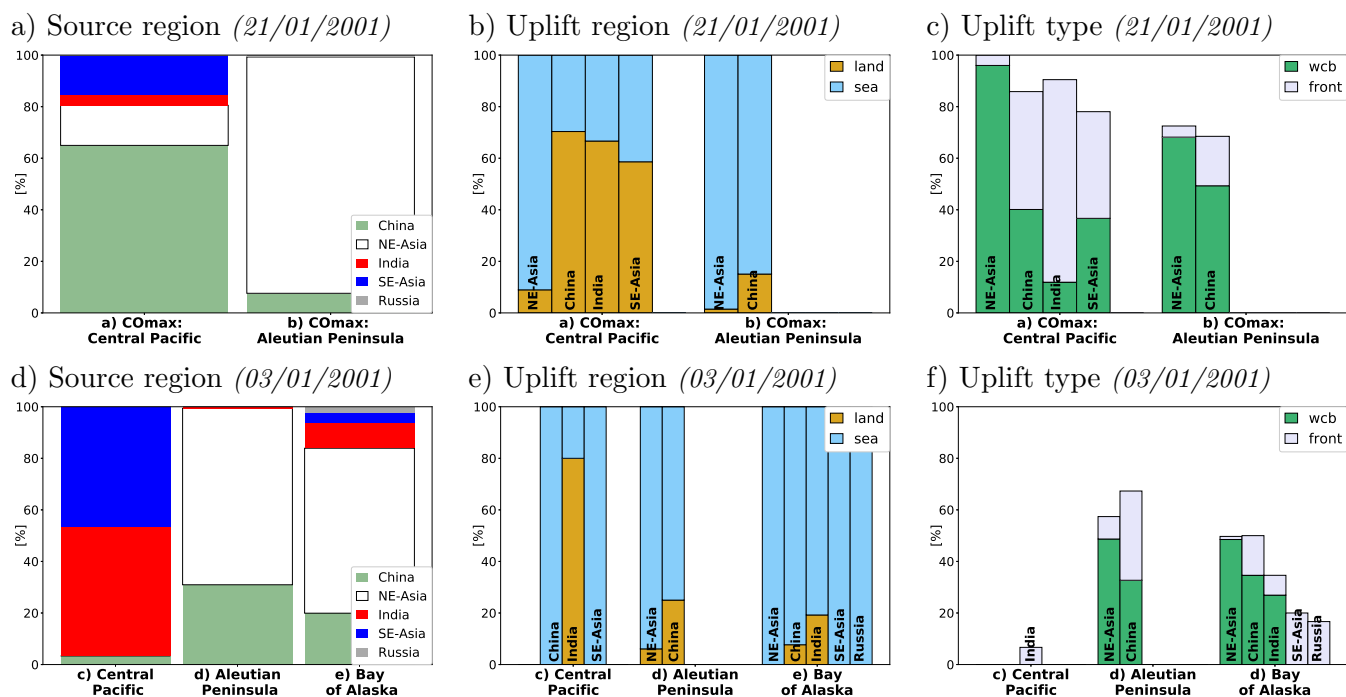

Figure 6. Plots show statistics for both case study days. The x-axis label refers to the different CO maxima cluster shown if Fig. 5. Source regions are shown in Fig. 8 a.

3.2 Transport characteristics

One of the questions we address in this study is the potential importance of vertical transport of pollution by extratrocpical cyclones and particularly warm conveyor belts as part of long-range transport events. Closely following Madonna et al. (2014), we define a criterion for ~~wcb~~ WCB related upward transport: trajectories must be located within a two-dimensional surface cyclone field for at least one 6-hourly time step during the ascend phase. i.e. trajectories must cross the cyclone within the time between two time steps prior or after the lift above the 800hPa level (Fig. 8).

This condition does not only ensure that trajectories rise in the vicinity of a cyclone but it also excludes accidental consideration of convectively uplifted air masses (Madonna et al., 2014). We require uplift from below 800hPa to 400hPa (the altitude we mainly analyse, see section 2.2) but we give no time limit for the uplift. Our analysis reveals however, that by far the majority of all trajectories is lifted to 400hPa within 48 hours which is the time frame for ~~wcb-type~~ WCB-type uplift used in the study by Madonna et al. (2014).

To define the position and size of a cyclone we follow the method of Wernli and Schwierz (2006) and the modifications described by Madonna et al. (2014): Based on ERA-INTERIM reanalysis data a cyclone centre is defined as a local minimum in the sea level pressure. Starting at the centre of a cyclone, closed isobars are calculated in intervals of 0.5 hPa. To define the horizontal extension of a cyclone, this procedure is repeated until no closed isobars can be found. Like described by Madonna et al. (2014) our algorithm also allows the merging of two cyclones which are very close to each other. The algorithm calculating the horizontal extension of a cyclone tends to ~~rather underestimate~~ underestimate rather than overestimate the size of a cyclone.

In addition to ~~wcb~~ WCB type uplift, we determine trajectories being lifted along a frontal zone. The classification of trajectories belonging to this category follows the procedure described above but trajectories must cross a frontal zone during their ascent. The definition of a front follows in general one of the approaches discussed by Schemm et al. (2017): a frontal zone is identified by enhanced θ_e gradients (at least 4K/100km). We slightly modified this criterion by requiring a gradient of at least 3K in one grid box (0.75°) in the ERA-INTERIM data set. As discussed by Thomas and Schultz (2018) numerous definitions to detect a front in a gridded data set exist, all of them having their advantages and disadvantages. As the definition of the front has a rather high uncertainty and as the ERA-INTERIM data set has a rather coarse horizontal resolution of 0.75° it is likely that we miss frontal systems in our analysis. Therefore several trajectories do not fulfil one of the two above described criteria and are classified as 'rest'. Also trajectories which are orographically lifted belong to this group. Due to the coarse vertical resolution of the ERA-INTERIM data set which also underlays the MPTRAC trajectory calculations, it is not possible to separate those trajectories accurately.

The ERA-INTERIM based MPTRAC simulations do not explicitly represent deep convection since trajectory calculations are only driven by large scale wind fields. Therefore we cannot further distinguish between different uplift types occurring in the vicinity of a frontal zone. Due to the long simulation period of 19 years it is also not possible to analyse each uplift event individually as done by Liang et al. (2005). However, Lawrence and Salzmann (2008) point out that trajectories should represent the net vertical and long-range transport reasonably, since much of the convective upwelling in our region of interest

is connected to large scale circulations. As Lawrence and Salzmann (2008) and Lawrence and Lelieveld (2010) discuss in detail, it can be assumed that the basic regional lofting will be present in lagrangian trajectory simulations using input from global circulation models. ~~Though it can~~ It has to be expected that the mean rate of vertical transport is underestimated.

4 ~~Results~~

3.1 ~~CO enhancements observed by MOPITT~~

~~lSeasonal mean CO mixing ratios ppbfrom MOPITT at 400hPa including all available data points (2000-2019). Plots in the bottom row show daily CO mixing ratios from MOPITT for two selected days. Black crosses (bottom row) mark the 2% highest CO values of the given day, which are selected. Black squares mark the region in which trajectories are initiated. In order to investigate the impact of the continental Asian outflow on mid- and upper tropospheric pollution level, we analyse CO data from MOPITT on different pressure level. As mentioned above, we only include the highest 2% of all daily available data points for each level in our analysis. We refer to them as CO-maxima events. As we are primarily interested in upper tropospheric pollution episodes, we focus our analysis on the 400hPa data from MOPITT. We also detect regularly CO-maxima events over the NH-Pacific at 500hPa and 300hPa. Though during winter time, no clear CO-maxima signal is visible over the northern Pacific at 300hPa. North of about 45°, the 300hPa level is frequently located above the tropopause during winter (Wilcox et al., 2012) where CO mixing ratios decrease quickly.Figure 1 (upper and centre row) shows seasonal mean CO mixing ratios from 2000-2019 at 400hPa, including all available level 3-MOPITT data points. Throughout the year, CO mixing ratios over the NH-Pacific belong to the highest mixing ratios observed globally, especially during winter, spring and summer. During autumn mixing ratios are high over typical biomass burning regions (South America, southern Africa) and their outflow regions over the southern hemispheric Pacific and Indian Ocean.To identify individual synoptic scale pollution events and analyse them individually, we filter MOPITT data as described above. By only using 2% of all daily available data points we include roughly 80-130 grid points per day in our analysis (black crosses, Fig. 1, bottom row). As we select those grid points, independently where they are, it is hypothetically possible that on days with strong and widespread biomass burning at any region outside the studying region, the pollution signal over the NH-Pacific is weak and we underestimate the number of severe pollution events. Though, due to the incomplete global coverage of the satellite data, MOPITT only sees a fraction of the potential biomass burning area (Fig. 1, bottom row). The situation is only different during autumn when CO mixing ratios over southern Africa and America are extraordinary high and the biomass burning CO-signal is visible broadly over the southern hemispheric Atlantic and Indian Ocean (Fig. 1, SON). Indeed, we detect much less pollution events over the NH-Pacific during this time of the year (Fig. 3 SON) but, CO mixing ratios there are much lower during autumn than during the rest of the year.lDifference (in ppb) between CO seasonal mean mixing ratios considering only CO-maxima events and total seasonal mean CO mixing ratios including all valid data points (2000-2019). Grid points which are marked by grey crosses have a difference with a strong statistical significance (regions where the pooled standard deviation is within a 99% confidence interval). In general, CO-maxima events represent periods of elevated CO mixing ratios compared to background level. The difference between mean CO mixing ratios considering only CO-maxima events and mean CO mixing ratios considering all~~

12

data is rather high over almost the entire NH-Pacific during all seasons (Fig. 2). This indicates, that by our selection of data points we really capture periods with extraordinary high pollution level in the upper troposphere. An exception is clearly visible over the northern Pacific during winter (Fig. 2, DJF) where the difference in CO mixing ratios is rather small and of no statistical significance. CO maxima events occur regularly in this region, though not significantly more often than over the central NH-Pacific where the difference in CO mixing ratios between both data sets is much larger. Thus we can assume that CO level prevailing while the grid points were selected as a maximum, represent rather the climatological mean than a single extreme event. This conclusion can also be drawn for the central NH-Pacific during spring (Fig. 2, MAM). Regions with a difference in CO mixing ratios of low statistical significance are also found during summer east of Japan (Fig. 2, JJA) where many maxima events occur. Though, this region is much closer to potential CO sources than the northern/central Pacific. Thus it is less surprising that pollution outflow events strongly impact the overall climatological mean at this site.High CO level occur throughout the year over the NH-Pacific with autumn showing an exception with much less events than during the rest of the year (Fig. 3). A seasonal shift of the regions where most CO maxima occur at 400hPa is clearly visible (also at 500hPa and 300hPa). In winter time (Fig. 3, DJF), CO-maxima occur more often over the north-eastern Pacific while they are found over the central NH-Pacific during spring (Fig. 3, MAM). The total number of CO-maxima events is much higher during spring than in other seasons. This agrees with other studies showing enhanced pollution export from Asia during spring (e.g. Luan and Jaeglé, 2013; Holzer et al., 2005; Zhang et al., 2008; Yu et al., 2008; Liang et al., 2004). During summer time (JJA) the passage of midlatitude cyclones is generally less frequent than during winter and spring while convection and the Asian summer monsoon gain in importance as transport pathways. The detected CO maxima are then found much closer to the continent over the western NH-Pacific, Siberia and Kamchatka.lNumber of CO-maxima events at a particular grid point for each season (winter (DJF), spring (MAM), summer (JJA) and autumn (SON)), summed up over the years 2000-2019. Only CO-maxima in the area which is not grey-shaded is included in the trend- and trajectory analysis. The total number of CO-maxima events at a particular grid point over the NH-Pacific does not seem to be exceptionally high (Fig. 3). Many grid points are only selected 10-15 times as a CO-maximum point within one season in 20 years. On the example day shown (03.01.2001) we detect three CO-maxima cluster over the NH-Pacific (marked by black squares) consisting of 12, 18 and 12 grid points (Fig. 1). The small number of total counts of each single grid point is (i) the consequence of the incomplete spatial coverage of MOPITT (Fig. 1, bottom row), (ii) the rather high spatial variability of the position of the CO-maximum cluster and (iii) the rather small number of grid points which we select daily. The number of valid data points over the northern Pacific is smaller than over other parts of the world (mainly due to clouds, Fig. 1, bottom row). lPlots in the left column show time series of the season mean number of daily CO-maxima grid points, normalised with the total number of valid MOPITT data points. Circles are coloured with the ENSO index (taken from https://www.cpc.ncep.noaa.gov/products). Vertical lines show the standard deviation of the daily number of CO-maxima grid points with respect to the season mean. Plots in the centre column show the season mean number of daily CO-maxima cluster and plots in the right column show the percentage of the number of CO-maxima days within one season. Excluded from the statistics are CO-maxima over the continent and coastal areas close to major CO source regions (grey area marked in Fig. 3 not included). For the trend calculation, MOPITT data until 03/2020 are included. Nevertheless, we detect CO-maxima over the NH-Pacific during ∼ 70% of all days during winter and

summer and ~ 80% during spring (Fig. 4 right column). The number of grid points which are selected as a CO-maximum each day varies however, strongly (visible in the high standard deviation, Fig. 4 left column). During winter, the mean number of grid points which we select as CO-maxima, stays in the same order of magnitude throughout the 20 years of available MOPITT data. Though during spring it increases from 2000 until 2020 and decreases during summer (Fig. 4 left column). At the same time, the total number of valid MOPITT grid points increases/decreases. To account for this effect, we show the seasonal fraction of CO-maxima grid points with respect to the total number of valid MOPITT grid points over the NH-Pacific (Fig. 4 left column). Still, the increasing/decreasing trend is visible. Both trends (MAM, JJA) are mathematically of statistical significance. Though the results need to be carefully interpreted. At first, the standard deviation of the mean number of CO-maxima grid points found in one season is very high. Secondly, we cannot directly conclude, that the spatial coverage of severe pollution episodes increased, though it is likely. An increase of the number of CO-maxima grid points over the Pacific during spring could hypothetically be also the result of e.g.: (i) weaker biomass burning in other regions of the world, (ii) a faster dilution of biomass burning plumes, (iii) less clouds over the Pacific or more clouds over other polluted areas or (iv) instrumentational reasons. Since precipitation patterns over the Pacific and the position of the jet stream can be altered during El Niño episodes (Breeden et al., 2021), and thus transport pathways of pollution plumes, we considered a correlation between warm phases of ENSO and severe pollution episodes. Years with an extraordinary large spatial extension of the upper tropospheric pollution plumes (e.g. 2004, 2009, 2016, 2019) are indeed related with El Niño periods (Fig. 4 left column). This conclusion can however, only be drawn for spring and is in agreement with the work by Breeden et al. (2021) who find an increase in storm track activity during La Niña years compared to neutral or El Niño years.The number of days on which we detect CO-maxima does not show a corresponding positive trend during spring (Fig. 4 right column, MAM). The percentage of CO-maxima days during spring is even lower between 2010-2019 compared to the years 2003-2009. During winter, summer and autumn the number of CO-maxima days shows a decreasing trend corresponding to the decreasing trend in the number of CO-maxima grid points. Though the linearity of the the data set is rather weak (Fig. 4 right column, DJF, JJA, SON) and therefore the trend. We also calculated the season mean number of CO-maxima cluster (Fig. 4 centre column) which however, does not change significantly during spring leading to the conclusion that the spatial coverage of individual pollution cluster increases in spring during the 20 years we analysed.lPlots show trajectories starting at a CO-maxima cluster on 03.01.2001 (lower row) and 21.01.2001 (upper row). Trajectories with the same source region, have the same colour (see legend, e.g. trajectories from China are green, those from SE-Asia blue). The lighter the colour of the circles marking the position of the trajectory, the lower the pressure level. Yellow circles mark the time of uplift, black circles (over the Pacific) mark the start position of the trajectories, i.e. the region of the CO-maxima cluster. lPlots show statistics for both case study days. The x-axis label refers to the different CO-maxima cluster shown if Fig. 5. Source regions are shown in Fig. 8 a.

14

4 ~~Specification of CO emission regions~~

3.1 Case study

As described in section 3.1, we use lagrangian trajectory calculations and ERA-INTERIM reanalysis data to analyse the source regions of upper tropospheric CO detected over the Pacific and related uplift mechanisms. To better illustrate the trajectory analysis, we will discuss in more detail two particular days (03.01.2001, 21.01.2001) with ~~CO-maxima~~ CO maxima being

330 observed over the remote Pacific by MOPITT (Fig. 5). On both days a CO-maximum cluster was found near the Aleutian peninsula (Fig. 5 b,d) and over the central NH-Pacific (Fig. 5 a,c). On 03.01, a third cluster was found over the gulf of Alaska (Fig. 5 e).

Trajectory simulations link all three ~~CO-maxima~~ CO maxima cluster north of ~~30~~40°N (Fig. 5 ,b,d,e~~, Fig. 6 ,a,d)~~) mainly with NE-Asia (dark red trajectories) and NE-China (green trajectories) as source regions while the cluster over the central NH-

335 Pacific (Fig. 5 a,c) ~~have~~ has a strong contribution from air masses coming from (SE-)China (green trajectories)~~in addition to air masses coming from~~, SE-Asia (blue trajectories) and India (orange trajectories). Even though both ~~cluster~~ clusters over the central NH-Pacific are found in very similar regions ($\sim$ 170°E, 30°N, Fig. 5 a,c), trajectory simulations indicate significantly different source regions: On 21.01 (Fig. 5 a, Fig. 6 a), 65% of all trajectories come from China, 15% from NE-Asia and SE-Asia and a small fraction of trajectories come from India (4%). While the CO maximum observed on 03.01 (Fig. 6 d) is mainly fed

340 with CO from SE-Asia (46% of all trajectories) and India (50%) while China seems to play a minor role as source region (3%) on that particular day.

Most of the trajectories reaching the CO maximum over the Aleutian peninsula on 21 January, are lifted into the free troposphere in the vicinity of an eastward moving cyclone (66% of all trajectories, Fig.5 b, Fig.6 c). Fig.7 shows exemplarily the position of the cyclone at 18:00 UTC, 14.01.2001 (a) and 00:00 UTC on 15.01.2001 (b). Once being lifted into the free

345 troposphere, air masses are transported north-eastward, circulate in the Aleutian low, and finally move further north towards the Arctic or eastward towards the American west coast (not shown). ~~Thus long range transport of polluted air masses to the northern CO-cluster on 21 January~~ This transport pathway is typical of LRT by fast uplift of air masses in the warm conveyor belt of a midlatitude cyclone over the Pacific with subsequent eastward motion in the free troposphere (Madonna et al., 2014). In contrast, air masses reaching the second cluster on 21 January over the central NH-Pacific (Fig.5 a) are mainly lifted into the

350 free troposphere over the continent (Fig. 6 b,c) along a front.

Air masses reaching the CO-maximum cluster over the Aleutian peninsula on 03 January do not show such a uniform transport pattern as seen on 21 January. Even though a large fraction of trajectories experience ~~web-type~~ WCB-type uplift (43% of all trajectories, Fig.6 d), the uplift time and uplift position has a stronger temporal and spatial variability compared to 21 January. Air masses need on average 3.3 days to reach the ~~CO-maxima~~ CO maxima cluster after rise into the free troposphere (4.8 days

355 on 21.01.). Parts of the air masses are lifted faster to higher altitudes ($\sim$ 400hPa 6-12 hours after uplift, Fig. 7 e, trajectories at the edge of the cyclone at $\sim$ 165°E), compared to 21 January, but transport patterns in the free troposphere are rather diffuse (Fig.7 d,e). On both case study days, a strong Aleutian low has built up. Though ~~it~~ its position differs on both days. It is located over the gulf of Alaska on 03 January (Fig.7 f) and over the Aleutian peninsula on 21 January (Fig.7 c).

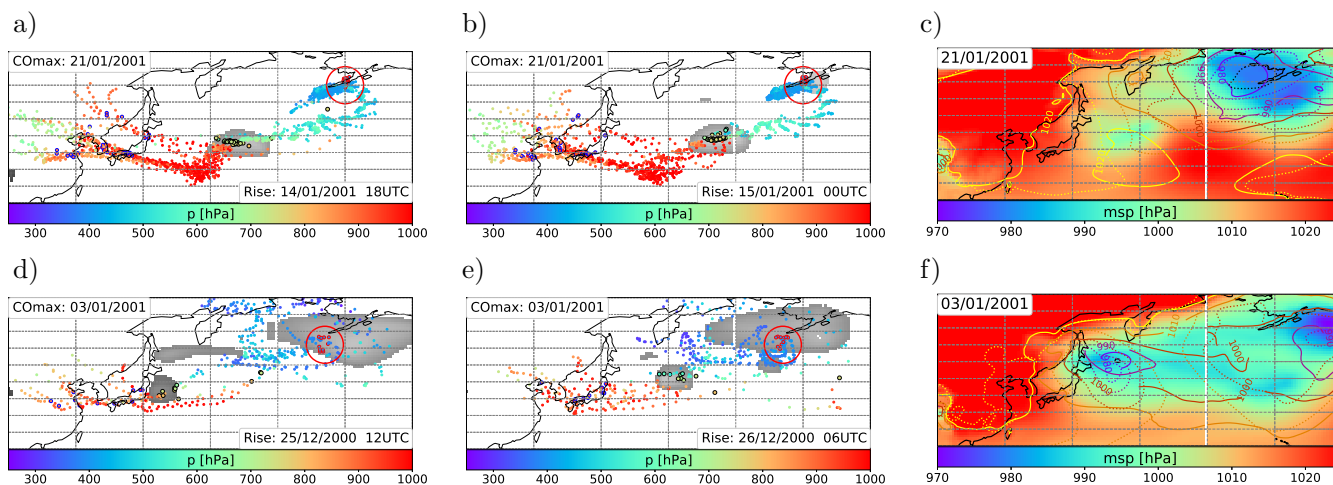**Figure 7.** Plots (a-b),(d-e) show trajectories reaching a common ~~CO-maxima~~ CO maxima cluster and having a common time of rise (above 800hPa). Black circles mark the trajectory position at the time of rise, blue circles mark the position of descend below 800hPa above a CO emission region. Grey shaded areas mark the position of a low pressure system in the ERA-interim data set. Plots c) and f) show a daily average of the mean sea level pressure [hpa] taken from ERA-interim on 21.01.2001 (c) and 03.01.2001 (f). Solid contour lines show the daily mean msp one day prior the case study day (20.01.2001 (c), 02.01.2001 (f)) and dotted contour lines two days prior the case study day (19.01.2001 (c), 01.01.2001 (f)).

The ~~pollution plume~~ CO maxima cluster over the gulf of Alaska (Fig. 5 e) is half composed of air masses which were lifted along a front near CO emission regions (NE-China, NE-Asia) and eastward transport took place in the free troposphere while the other half crossed almost the entire Pacific in the lower most (marine) troposphere. Those air masses are finally lifted into the free troposphere close to the observed CO-maximum cluster in the vicinity of a cyclone. As a consequence it can be assumed that both plume composites experience significantly different chemical processing and mixing during transport.

3.2 Statistics of long-term observational data set (2000-2018)

We extended the above presented statistics to all ~~CO-maxima~~ CO maxima cluster detected in our simulation period (03/2000-12/2018) and to all trajectories being calculated for each single CO-maximum cluster. As described in section 3.1, backward trajectories are assigned to a certain source region, if they descend below 850hpa, are less than 1.5 km above ground and CO emissions exceed a certain threshold. Throughout the year, trajectories reveal China as the dominant source region (Fig. 8 d) of upper tropospheric CO. The contribution of other regions shows a stronger seasonality: during winter and summer almost the same percentage of trajectories come from NE-Asia (33.7% DJF, 27.9% JJA) as from China (36.8% DJF, 29% JJA, Fig. 8 d). During spring however, India becomes an important upper tropospheric CO source region (32% source contribution). During summer the total percentage of trajectories coming from India is smaller than during spring. Though, we find that the individual contribution of India to a single pollution event is stronger during summer than during spring.

Considering only ~~CO-maxima~~ CO maxima over the NE-Pacific (north of 45 °N, Fig. 8 e), China and NE-Asia are the dominant
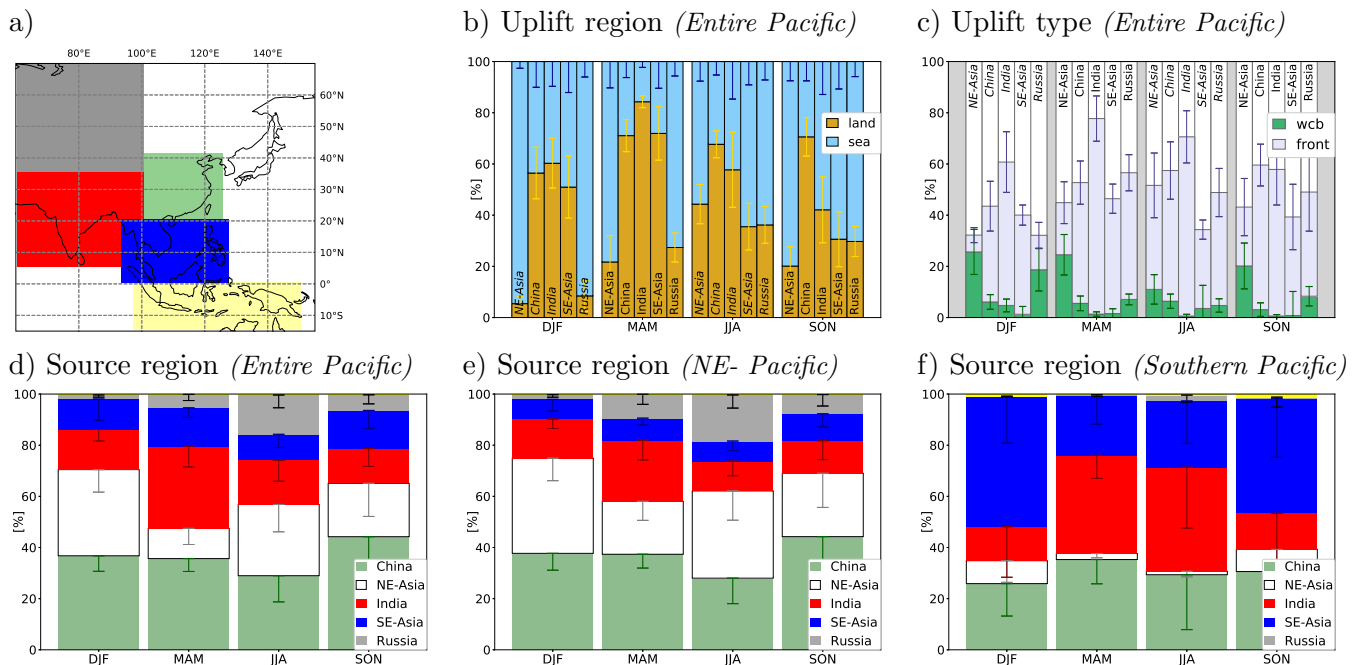
16

Figure 8. ~~Source~~ CO source regions ~~between which we distinguish~~ are shown in (a): China (green), NE-Asia (white), India (red), SE-Asia (blue), Russia (grey), and Indonesia (yellow). The contribution from Indonesia is very small and almost not visible in the bar charts. All other plots show seasonal statistics (in [%]) of the trajectory calculations: Fig.8(b) shows the percentage of trajectories rising over land or sea in dependency on the source region. The uplift type is shown in (c). Plots (d-f) show the percentage of trajectories coming from a particular source region (i) including all ~~CO-maxima~~ CO maxima over the entire Pacific (d), (ii) including only ~~CO-maxima~~ CO maxima north of 45 °N (e) and (iii) including ~~CO-maxima~~ CO maxima only between 0° and 30°N (f). Vertical lines show the standard deviation (only plotted in the negative direction in plots (d-f)).

375 CO source regions (statistics are similar as for the entire Pacific). Though, only considering ~~CO-maxima~~ CO maxima over the southern NH-Pacific (between 0° and 30°N), we see a much stronger source contribution from SE-Asia (Fig. 8 f), especially during winter (50%) and autumn (45%) and respectively India during spring (38.4%) and summer (40.7%).

The yellow area marked in Fig. 8 a) covering Indonesia, has a source region contribution of less than 1% and is therefore (almost) not visible in the bar charts in Fig. 8.

380 ~~The two case studies indicates~~Both case studies presented above indicate, that pollution plumes reaching a CO-maximum over the NE-Pacific during winter coming from NE-Asia ~~, are often~~ and are predominantly lifted into the free troposphere in the warm conveyor belt of a mid-latitude cyclone over the Pacific. Statistics including all 19 years of trajectory calculations ~~lead to the same~~ confirm this result: More than 90% of all trajectories from NE-Asia ~~rise over sea~~ ascend over the ocean during winter (almost 80% during spring) (Fig. 8 b, DJF) and 26% of these trajectories rise by ~~wcb-type~~ WCB-type uplift (Fig. 8 c,

385 DJF). ~~Only taking those trajectories as a measure for which we can determine the type of rise, more than~~ We found, that 90% of ~~those~~ the trajectories, which fit our criteria of vertical transport, are classified as ~~wcb-type~~WCB-type.

The fraction of ~~wcb-related~~ WCB-related upward transport is much smaller for all other source regions throughout the year. This finding is in agreement with the detailed study by Madonna et al. (2014) who show that by far the largest fraction of trajectories experiencing ~~web-type~~ WCB-type uplift over the Pacific come from NE-Asia especially during winter. This can

390 be explained with the position of a semi permanent low pressure system over Japan during winter time (Liang et al., 2005; Madonna et al., 2014). For trajectories from all other source regions, uplift along a front line is the dominant uplift process. The uplift region shows a strong seasonality for all source regions. Only trajectories coming from China are predominantly lifted over land throughout the year (more than 60% with a rather small standard deviation, Fig. 8 b).

The time between rise into the free troposphere and the arrival of air masses at the CO cluster is longer for trajectories coming

395 from China (3.7 days DJF, 6.6 days JJA), compared to NE-Asia (2.8 days DJF, 5.7 days JJA) corresponding to different uplift regions (land/sea). The residence time in the free troposphere is longer in summer than in winter for all source regions even though CO maxima are located much closer to the continent during summer compared to winter. It is not surprising that trajectories coming from India have the longest residence time in the free troposphere before reaching the CO maxima site (6.5 days DJF, 9 days JJA).

400 ## 4 Conclusions

~~We analysed~~ By analysing the global distribution of the highest 2% of daily CO mixing ratios at 400hPa derived from MOPITT for 20 ~~years of CO data from the MOPITT satellite instrument with a particular focus on long-range transport of Asian pollution to the extratropical upper troposphere~~ years, we (i) detect very regularly regions with very high CO mixing ratios (i.e. belonging to the globally highest 2% values) over the remote NH-Pacific. ~~Our study indicates that those long-range transport events occur~~

405 ~~regularly and with a high frequency in particular during winter and spring (on average more than one long-range transport event per week during spring and roughly one event per week during~~ Based on an extended analysis of lagrangian trajectories in combination with ERA-INTERIM data, we (ii) conclude that long range transport events from east Asia are responsible for the observed CO maxima. We (iii) can link the majority of CO maxima not only to a specific source region but also with a distinct transport and uplift mechanism.

410 In agreement with the findings by Luan and Jaeglé (2013); Liang et al. (2004, 2005, 2007) we see a strong seasonality of pollution events over the Pacific with most CO maxima being observed during spring, followed by winter and summer~~). Additionally, the spatial coverage of upper tropospheric CO-plumes seams to increase during spring within the 20 years of analysed data. We find that regions where most CO-maxima occur show a strong seasonal cycle~~. Our results further extend the conclusion of these authors since we analysed the effect of LRT and vertical transport on the composition of the upper troposphere region.

415 Notably, we see a spatial shift of the occurrence of the CO maxima related to different transport pathways with most events being detected over the north-eastern Pacific during winter, over the central NH-Pacific during spring and over the western NH-Pacific during summer.~~This shift of pollution patterns indicates significantly different transport pathways depending on the season. In addition, the~~

The contribution of different CO emission regions to the observed upper tropospheric CO plumes change among the seasons.

420 Though China is the major CO source region throughout the year. In relation with uplift in the warm conveyor belt of a midlatitude cyclone, NE-Asia is the second most important source region for upper tropospheric CO observed over the north-eastern Pacific in particular during winter.

~~The statistical analysis of our trajectory simulations reveal~~ In general, we find a correlation between ~~certain CO source regions,~~

~~uplift types, uplift region and upper tropospheric pollution regions. Thougha more detailed analysis of single case studies,~~

425 ~~reveal that the transport time of air masses reaching one single CO-maximum can differ strongly~~ the occurrence of high levels of CO in the upper troposphere over the remote Pacific (e.g. over the Aleutian peninsula/north-eastern NH-Pacific during winter) and the synoptic situation. We identified common uplift mechanisms for trajectories having a common source region and a common start region (thus the region where CO maxima are found). Though, we find strong differences when comparing in detail individual pollution events with each other (regarding: location of CO maxima, location, strength and development of

430 the Aleutian low, transport time from a CO-source region over the continent to the observation location of elevated CO over the Pacific, location of uplift from the boundary layer to the upper troposphere, position and strength of cyclones leading to uplift, residence time in the boundary layer/free troposphere during transport). Even though we describe transport patterns for one of our case studies (21.01.2001, ~~CO-max~~ CO maxima cluster over the Aleutian Peninsula) as rather uniform, the time of uplift of air masses in the vicinity of a midlatitude cyclone into the free troposphere differs by more than 24 hours for single trajectories,

435 corresponding to hundreds of kilometres in distance. ~~Therefore, it is almost impossible to create composites of similar events in order to define transport regimes in relation to the prevailing synoptic situation, source region and upper tropospheric pollution location.In general, the time between rise into the free troposphere and the arrival of air masses at the CO cluster is longer for trajectories coming from China (3.7 days DJF, 6.6 days JJA), compared to NE-Asia (2.8 days DJF, 5.7 days JJA) corresponding to different uplift regions (land/sea). The residence time in the free troposphere is longer in summer than in winter for all source~~

440 ~~regions even though CO-maxima are found much closer to the continent during summer compared to winter. It is not surprising that trajectories coming from India have the longest residence time in the free troposphere before reaching the CO-maxima site (6.5 days DJF, 9 days JJA). As a consequence of different transport patterns we can assume that the chemical composition and processing of Asian pollution plumes differs significantly depending on the source region and transport pathway~~ This is due to the fact, that the relevant synoptic systems may exist for several hours or days thereby travelling over large distances which

445 results in a broad temporal and spatial range between source emission and vertical uplift of potential polluted air masses.

The observations of CO maxima at 400hPa ~~confirms~~ confirm the crucial role of east Asian emissions for the pollution of the lower UTLS. Notably this also holds for non-monsoon seasons. Our analysis presents evidence for a surprisingly regular and highly frequent occurrence of these long-range transport events. Taking CO as a general marker of pollution and given the regularity of the transport processes, our study highlights the global role of the region also for other chemical constituents in

450 the upper troposphere.

References

460   Bey, I., Jacob, D. J., Logan, J. A., and Yantosca, R. M.: Asian chemical outflow to the Pacific in spring: Origins, pathways, and budgets, Journal of Geophysical Research: Atmospheres, 106, 23 097–23 113, https://doi.org/10.1029/2001JD000806, 2001.

Breeden, M. L., Butler, A. H., Albers, J. R., Sprenger, M., and Langford, A. O.: The spring transition of the North Pacific jet and its relation to deep stratosphere-to-troposphere mass transport over western North America, Atmospheric Chemistry and Physics, 21, 2781–2794, https://doi.org/10.5194/acp-21-2781-2021, 2021.

465   Chen, Y., Zhao, C., Qiang, Z., Deng, Z., Huang, M., and Ma, X.: Aircraft study of Mountain Chimney Effect of Beijing, China, Journal of Geophysical Research, 114, 1–10, https://doi.org/10.1029/2008JD010610, 2009.

Dee, D. P., Uppala, S. M., Simmons, A. J., Berrisford, P., Poli, P., Kobayashi, S., Andrae, U., Balmaseda, M. A., Balsamo, G., Bauer, P., Bechtold, P., Beljaars, A. C. M., van de Berg, L., Bidlot, J., Bormann, N., Delsol, C., Dragani, R., Fuentes, M., Geer, A. J., Haimberger, L., Healy, S. B., Hersbach, H., Hólm, E. V., Isaksen, L., Kållberg, P., Köhler, M., Matricardi, M., McNally, A. P., Monge-Sanz,

470   B. M., Morcrette, J.-J., Park, B.-K., Peubey, C., de Rosnay, P., Tavolato, C., Thépaut, J.-N., and Vitart, F.: The ERA-Interim reanalysis: configuration and performance of the data assimilation system, Quarterly Journal of the Royal Meteorological Society, 137, 553–597, https://doi.org/https://doi.org/10.1002/qj.828, 2011.

Deeter, M., Edwards, D., Gille, J., and Worden, H.: Information content of MOPITT CO profile retrievals: Temporal and geographical variability, Journal of Geophysical Research: Atmospheres, 120, n/a–n/a, https://doi.org/10.1002/2015JD024024, 2015.

475   Deeter, M., Edwards, D., Gille, J., Mao, D., Martínez-Alonso, S., Worden, H., Ziskin, D., and Andreae, M.: Radiance-based retrieval bias mitigation for the MOPITT instrument: the version 8 product, Atmospheric Measurement Techniques, 12, 4561–4580, https://doi.org/10.5194/amt-12-4561-2019, 2019.

Di Pierro, M., Jaeglé, L., and Anderson, T. L.: Satellite observations of aerosol transport from East Asia to the Arctic: three case studies, Atmospheric Chemistry and Physics, 11, 2225–2243, https://doi.org/10.5194/acp-11-2225-2011, 2011.

480   Dickerson, R., Li, C., Li, Z., Marufu, L., Stehr, J., McClure, B., Krotkov, N., Chen, H., Wang, P., Xia, X., Ban, X., and Gong, F.: Aircraft Observations of Dust and Pollutants over NE China: Insight into the Meteorological Mechanisms of Long-Range Transport, Journal of Geophysical Research, 112, https://doi.org/10.1029/2007JD008999, 2007.

Ding, A., Wang, T., Xue, L., Gao, J., Stohl, A., Lei, H., Jin, D., Ren, Y., Wang, X., Wei, X., Qi, Y., Liu, J., and Zhang, X.: Transport of north China air pollution by midlatitude cyclones: Case study of aircraft measurements in summer 2007, Journal of Geophysical Research:

485   Atmospheres, 114, https://doi.org/https://doi.org/10.1029/2008JD011023, 2009.

Ding, K., Liu, J., Ding, A., Liu, Q., Zhao, T., Shi, J., Han, Y., Wang, H., and Jiang, F.: Uplifting of carbon monoxide from biomass burning and anthropogenic sources to the free troposphere in East Asia, Atmospheric Chemistry and Physics, 15, 2843–2866, https://doi.org/10.5194/acp-15-2843-2015, 2015.

Eckhardt, S., Stohl, A., Wernli, H., James, P., Forster, C., and Spichtinger, N.: A 15-Year Climatology of Warm Conveyor Belts, Journal of

490   Climate, 17, 218–237, 2004.

Fuelberg, H., Hannan, J., Crawford, J., Sachse, G., and Blake, D.: The Role of Wave Cyclones in Transporting Boundary Layer Air to the Free Troposphere During the Spring 2001 NASA / TRACE-P Experiment, Journal of Geophysical Research D: Atmospheres, 108, https://doi.org/10.1029/2002JD003105, 2003.

Garny, H. and Randel, W. J.: Transport pathways from the Asian monsoon anticyclone to the stratosphere, Atmospheric Chemistry and

495   Physics, 16, 2703–2718, https://doi.org/10.5194/acp-16-2703-2016, 2016.

Gehring, J., Oertel, A., Vignon, E., Jullien, N., Besic, N., and Berne, A.: Microphysics and dynamics of snowfall associated with a warm conveyor belt over Korea, Atmospheric Chemistry and Physics, 20, 7373–7392, https://doi.org/10.5194/acp-20-7373-2020, 2020.

Han, H., Liu, J., Yuan, H., Jiang, F., Zhu, Y., Wu, Y., Wang, T., and Zhuang, B.: Impacts of Synoptic Weather Patterns and their Persistency on Free Tropospheric Carbon Monoxide Concentrations and Outflow in Eastern China, Journal of Geophysical Research: Atmospheres, 123, https://doi.org/10.1029/2017JD028172, 2018.

Heald, C., Jacob, D., Fiore, A., Emmons, L., Gille, J., Deeter, M., Warner, J., Edwards, D., Crawford, J., Hamlin, A., Sachse, G., and Browell, E.: Asian outflow and trans-Pacific transport of carbon monoxide and ozone pollution: An integrated satellite, aircraft and model perspective, Journal of Geophysical Research, 108, https://doi.org/10.1029/2003JD003507, 2003.

Hoffmann, L., Rößler, T., Griessbach, S., Heng, Y., and Stein, O.: Lagrangian transport simulations of volcanic sulfur dioxide emissions: Impact of meteorological data products, Journal of Geophysical Research: Atmospheres, 121, 4651–4673, https://doi.org/10.1002/2015JD023749, 2016.

Holzer, M., Hall, T., and Stull, R.: Seasonality and weather-driven variability of transpacific transport, Journal of Geophysical Research, 110, https://doi.org/10.1029/2005JD006261, 2005.

Hu, Z., Huang, J., Zhao, C., Ma, Y., Jin, Q., Qian, Y., Leung, L. R., Bi, J., and Ma, J.: Trans-Pacific transport and evolution of aerosols: spatiotemporal characteristics and source contributions, Atmospheric Chemistry and Physics, 19, 12 709–12 730, https://doi.org/10.5194/acp-19-12709-2019, 2019.

Kaneyasu, N., Takeuchi, K., Hayashi, M., Fujita, S.-i., Uno, I., and Sasaki, H.: Outflow patterns of pollutants from East Asia to the North Pacific in the winter monsoon, Journal of Geophysical Research, 105, 17 361–17 378, https://doi.org/10.1029/2000JD900138, 2000.

Kiley, C. and Fuelberg, H.: An examination of summertime cyclone transport processes during Intercontinental Chemical Transport Experiment (INTEX-A), J. Geophys. Res, 111, 24–6, https://doi.org/10.1029/2006JD007115, 2006.

Klich, C. and Fuelberg, H.: The role of horizontal model resolution in assessing the transport of CO in a middle latitude cyclone using WRF-Chem, Atmospheric Chemistry and Physics, 14, https://doi.org/10.5194/acp-14-609-2014, 2014.

Knippertz, P. and Wernli, H.: A Lagrangian Climatology of Tropical Moisture Exports to the Northern Hemispheric Extratropics, Journal of Climate, 23, 987–1003, https://doi.org/10.1175/2009JCLI3333.1, 2010.

Lamarque, J.-F., Bond, T. C., Eyring, V., Granier, C., Heil, A., Klimont, Z., Lee, D., Liousse, C., Mieville, A., Owen, B., Schultz, M. G., Shindell, D., Smith, S. J., Stehfest, E., Van Aardenne, J., Cooper, O. R., Kainuma, M., Mahowald, N., McConnell, J. R., Naik, V., Riahi, K., and van Vuuren, D. P.: Historical (1850–2000) gridded anthropogenic and biomass burning emissions of reactive gases and aerosols: methodology and application, Atmospheric Chemistry and Physics, 10, 7017–7039, https://doi.org/10.5194/acp-10-7017-2010, 2010.

Lawrence, M. and Lelieveld, J.: Atmospheric pollutant outflow from southern Asia: a review, Atmospheric Chemistry and Physics Discussions, 10, https://doi.org/10.5194/acpd-10-9463-2010, 2010.

Lawrence, M. and Salzmann, M.: On interpreting studies of tracer transport by deep cumulus convection and its effects on atmospheric chemistry, ATMOSPHERIC CHEMISTRY AND PHYSICS, 8, https://doi.org/10.5194/acpd-8-12163-2008, 2008.

Lelieveld, J., Bourtsoukidis, E., Brühl, C., Fischer, H., Fuchs, H., Harder, H., Hofzumahaus, A., Holland, F., Marno, D., Neumaier, M., Pozzer, A., Schlager, H., Williams, J., Zahn, A., and Ziereis, H.: The South Asian monsoon—pollution pump and purifier, Science, 361, 270–273, https://doi.org/10.1126/science.aar2501, 2018.

Liang, Q., Jaeglé, L., Jaffe, D., Weiss, P., Heckman, A., and Snow, J.: Long-range transport of Asian pollution to the northeast Pacific: Seasonal variations and transport pathways of carbon monoxide, Journal of Geophysical Research, 109, https://doi.org/10.1029/2003JD004402, 2004.

Liang, Q., Jaeglé, L., and Wallace, J. M.: Meteorological indices for Asian outflow and transpacific transport on daily to interannual timescales, Journal of Geophysical Research: Atmospheres, 110, https://doi.org/10.1029/2005JD005788, 2005.

Liang, Q., Jaeglé, L., Hudman, R., Turquety, S., Jacob, D., Avery, M., Browell, E., Sachse, G., Blake, D., Brune, W., Ren, X., Cohen, R., Dibb, J., Fried, A., Fuelberg, H., Porter, M., Heikes, B., Huey, G., Singh, H., and Wennberg, P.: Summertime influence of Asian pollution in the free troposphere over North America, Journal of Geophysical Research: Atmospheres, 112, n/a–n/a, https://doi.org/10.1029/2006JD007919, 2007.

Liu, J., Drummond, J., Jones, D., Cao, Z., Bremer, H., Kar, J., Zou, J., Florian, N., and Gille, J.: Large horizontal gradients in atmospheric CO at the synoptic scale as seen by spaceborne Measurements of Pollution in the Troposphere, Journal of Geophysical Research, 111, https://doi.org/10.1029/2005JD006076, 2006.

Luan, Y. and Jaeglé, L.: Composite study of aerosol export events from East Asia and North America, Atmospheric Chemistry and Physics, 13, https://doi.org/10.5194/acp-13-1221-2013, 2013.

Madonna, E., Wernli, H., Joos, H., and Martius, O.: Warm Conveyor Belts in the ERA-Interim Dataset (1979–2010). Part I: Climatology and Potential Vorticity Evolution, Journal of Climate, 27, 3–26, https://doi.org/10.1175/JCLI-D-12-00720.1, 2014.

Matsui, H., Kondo, Y., Moteki, N., Takegawa, N., Sahu, L. K., Zhao, Y., Fuelberg, H. E., Sessions, W. R., Diskin, G., Blake, D. R., Wisthaler, A., and Koike, M.: Seasonal variation of the transport of black carbon aerosol from the Asian continent to the Arctic during the ARCTAS aircraft campaign, Journal of Geophysical Research: Atmospheres, 116, https://doi.org/10.1029/2010JD015067, 2011.

Müller, S., Hoor, P., Bozem, H., Gute, E., Vogel, B., Zahn, A., Bönisch, H., Keber, T., Krämer, M., Rolf, C., Riese, M., Schlager, H., and Engel, A.: Impact of the Asian monsoon on the extratropical lower stratosphere: trace gas observations during TACTS over Europe 2012, Atmospheric Chemistry and Physics, 16, 10 573–10 589, https://doi.org/10.5194/acp-16-10573-2016, 2016.

Ninomiya, K. and Shibagaki, Y.: Multi-Scale Features of the Meiyu-Baiu Front and Associated Precipitation Systems, Journal of The Meteorological Society of Japan - J METEOROL SOC JPN, 85B, 103–122, https://doi.org/10.2151/jmsj.85B.103, 2007.

Reidmiller, D. R., Jaffe, D. A., Fischer, E. V., and Finley, B.: Nitrogen oxides in the boundary layer and free troposphere at the Mt. Bachelor Observatory, Atmospheric Chemistry and Physics, 10, 6043–6062, https://doi.org/10.5194/acp-10-6043-2010, 2010.

Roiger, A., Schlager, H., Schäfler, A., Huntrieser, H., Scheibe, M., Aufmhoff, H., Cooper, O. R., Sodemann, H., Stohl, A., Burkhart, J., Lazzara, M., Schiller, C., Law, K. S., and Arnold, F.: In-situ observation of Asian pollution transported into the Arctic lowermost stratosphere, Atmospheric Chemistry and Physics, 11, 10 975–10 994, https://doi.org/10.5194/acp-11-10975-2011, 2011.

Santee, M. L., Manney, G. L., Livesey, N. J., Schwartz, M. J., Neu, J. L., and Read, W. G.: A comprehensive overview of the climatological composition of the Asian summer monsoon anticyclone based on 10 years of Aura Microwave Limb Sounder measurements, Journal of Geophysical Research: Atmospheres, 122, 5491–5514, https://doi.org/https://doi.org/10.1002/2016JD026408, 2017.

Schemm, S., Sprenger, M., and Wernli, H.: When during their life cycle are extratropical cyclones attended by fronts?, Bulletin of the American Meteorological Society, 99, https://doi.org/10.1175/BAMS-D-16-0261.1, 2017.

Thomas, C. and Schultz, D.: What are the Best Thermodynamic Quantity and Function to Define a Front in Gridded Model Output?, Bulletin of the American Meteorological Society, 100, https://doi.org/10.1175/BAMS-D-18-0137.1, 2018.

Tomsche, L., Pozzer, A., Ojha, N., Parchatka, U., Lelieveld, J., and Fischer, H.: Upper tropospheric CH_4 and CO affected by the South Asian summer monsoon during the Oxidation Mechanism Observations mission, Atmospheric Chemistry and Physics, 19, 1915–1939, https://doi.org/10.5194/acp-19-1915-2019, 2019.

Turquety, S., Clerbaux, C., Law, K., Coheur, P.-F., Cozic, A., Szopa, S., Hauglustaine, D., Hadji-Lazaro, J., Gloudemans, A., Schrijver, H., Boone, C., Bernath, P., and Edwards, D.: CO emission and export from Asia: an analysis combining complementary satellite measure-

ments (MOPITT, SCIAMACHY and ACE-FTS) with global modeling, Atmospheric Chemistry and Physics Discussions, 8, 1709–1755, https://doi.org/10.5194/acpd-8-1709-2008, 2008.

Vogel, B., Günther, G., Müller, R., Grooß, J.-U., Hoor, P., Krämer, M., Müller, S., Zahn, A., and Riese, M.: Fast transport from Southeast Asia boundary layer sources to northern Europe: rapid uplift in typhoons and eastward eddy shedding of the Asian monsoon anticyclone, Atmospheric Chemistry and Physics, 14, 12 745–12 762, https://doi.org/10.5194/acp-14-12745-2014, 2014.

Vogel, B., Günther, G., Müller, R., Grooß, J.-U., Afchine, A., Bozem, H., Hoor, P., Krämer, M., Müller, S., Riese, M., Rolf, C., Spelten, N., Stiller, G. P., Ungermann, J., and Zahn, A.: Long-range transport pathways of tropospheric source gases originating in Asia into the northern lower stratosphere during the Asian monsoon season 2012, Atmospheric Chemistry and Physics, 16, 15 301–15 325, https://doi.org/10.5194/acp-16-15301-2016, 2016.

Wernli, H.: A lagrangian-based analysis of extratropical cyclones. II: A detailed case-study, Quarterly Journal of the Royal Meteorological Society, 123, 1677–1706, https://doi.org/https://doi.org/10.1002/qj.49712354211, 1997.

Wernli, H. and Davies, H.: A Lagrangian-based analysis of extratropical cyclones. I: The method and some applications, Quarterly Journal of the Royal Meteorological Society, 123, 467 – 489, https://doi.org/10.1002/qj.49712353811, 1997.

Wernli, H. and Schwierz, C.: Surface Cyclones in the ERA-40 Dataset (1958–2001). Part I: Novel Identification Method and Global Climatology, Journal of the Atmospheric Sciences, 63, 2486–2507, https://doi.org/10.1175/JAS3766.1, 2006.

Wilcox, L., Hoskins, B., and Shine, K.: A global blended tropopause based on ERA data. Part I: Climatology, Quarterly Journal of the Royal Meteorological Society, 138, 561 – 575, https://doi.org/10.1002/qj.951, 2012.

Wuebbles, D. J., Lei, H., and Lin, J.: Intercontinental transport of aerosols and photochemical oxidants from Asia and its consequences, Environmental Pollution, 150, 65 – 84, https://doi.org/https://doi.org/10.1016/j.envpol.2007.06.066, 2007.

Yienger, J., Hastings, M., Holloway, T., Phadnis, M., Guttikunda, S., Carmichael, G., Moxim, W., and Levy, H.: The Episodic Nature of Air Pollution Transport From Asia to North America, Journal of Geophysical Research, 105, 26 931–26 946, https://doi.org/10.1029/2000JD900309, 2000.

Yihui, D. and Chan, J.: The East Asian summer monsoon: An overview, Meteorology and Atmospheric Physics, 89, 117–142, https://doi.org/10.1007/s00703-005-0125-z, 2005.

Yoon, J., Pozzer, A., Hoor, P., Chang, D. Y., Beirle, S., Wagner, T., Schloegl, S., Lelieveld, J., and Worden, H. M.: Technical Note: Temporal change in averaging kernels as a source of uncertainty in trend estimates of carbon monoxide retrieved from MOPITT, Atmospheric Chemistry and Physics, 13, 11 307–11 316, https://doi.org/10.5194/acp-13-11307-2013, 2013.

Yu, H., Remer, L., Chin, M., Bian, H., Kleidman, R., and Diehl, T.: A satellite-based assessment of transpacific transport of pollution aerosol, Journal of Geophysical Research, 113, https://doi.org/10.1029/2007JD009349, 2008.

Yu, P., Rosenlof, K. H., Liu, S., Telg, H., Thornberry, T. D., Rollins, A. W., Portmann, R. W., Bai, Z., Ray, E. A., Duan, Y., Pan, L. L., Toon, O. B., Bian, J., and Gao, R.-S.: Efficient transport of tropospheric aerosol into the stratosphere via the Asian summer monsoon anticyclone, Proceedings of the National Academy of Sciences, 114, 6972–6977, https://doi.org/10.1073/pnas.1701170114, 2017.

Yu, Y., Kalashnikova, O. V., Garay, M. J., and Notaro, M.: Climatology of Asian dust activation and transport potential based on MISR satellite observations and trajectory analysis, Atmospheric Chemistry and Physics, 19, 363–378, https://doi.org/10.5194/acp-19-363-2019, 2019.

Zhang, L., Jacob, D., Boersma, K., Jaffe, D., Olson, J., Bowman, K., Worden, J., Thompson, A., Avery, M., Cohen, R., Dibb, J., Flock, F., Fuelberg, H., Huey, L., Mcmillan, W., Singh, H., and Weinheimer, A.: Transpacific transport of ozone pollution and the effect of

recent Asian emission increases on air quality in North America: an integrated analysis using satellite, aircraft, ozonesonde, and surface observations, 2008.